JOC Article

# Tetrafullerene Conjugates for All-Organic Photovoltaics

Gustavo Fernández,[†] Luis Sánchez,[†] Dirk Veldman,[‡] Martijn M. Wienk,[‡] Carmen Atienza,[§] Dirk M. Guldi,*[,§] René A. J. Janssen,*[,‡] and Nazario Martín*[,†]

*Departamento de Química Orgánica, Facultad de Ciencias Químicas, Universidad Complutense de Madrid, Ciudad Universitaria s/n, 28040-Madrid, Spain, Molecular Materials and Nanosystems, Eindhoven University of Technology, 5600 MB Eindhoven, The Netherlands, and Department of Chemistry and Pharmacy and Interdisciplinary Center for Molecular Materials, Universität Erlangen-Nürnberg, Egerlandstrasse 3, 91058 Erlangen, Germany*

*nazmar@quim.ucm.es; r.a.j.janssen@tue.nl; dirk.guldi@chemie.uni-erlangen.de*

*Received January 8, 2008*

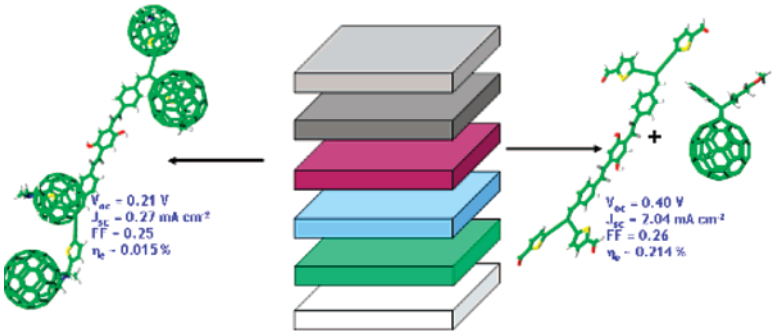


The synthesis of two new tetrafullerene nanoconjugates in which four $C_{60}$ units are covalently connected through different $\pi$-conjugated oligomers (oligo(*p*-phenylene ethynylene) and oligo(*p*-phenylene vinylene)) is described. The photovoltaic (PV) response of these $C_{60}$-based conjugates was evaluated by using them as the only active material in organic solar cells, showing a low PV performance. Photophysical studies in solution demonstrated a very fast (~10 ps) deactivation of the singlet excited state of the central core unit to produce both charge-separated species (i.e., $C_{60}^{\bullet-}$−oligomer$^{+\bullet}$−$(C_{60})_3$ and $C_{60}$ centered singlet excited states). The charge-separated state recombines partly to the $C_{60}$ centered singlet state that undergoes subsequent intersystem crossing. Photophysical studies carried out in films support these data, exhibiting long-lived triplet excited states. For both tetrafullerene arrays, the low yield of long-lived charge carriers in thin films accounts for the limited PV response. On the contrary, utilizing the oligo(*p*-phenylene vinylene) centered precursor aldehyde as an electron donor and antennae unit and mixing with the well-known $C_{60}$ derivative PCBM, the photophysical studies in films show the formation of long-lived charges. The PV devices constructed from these mixtures showed a relatively high photocurrent of 2 mA cm$^{-2}$. The sharp contrast between the nanoconjugates and the physical blends tentatively was attributed to improved charge dissociation and the collection of more favorable energy levels in the blends as a result of partial aggregation of both of the components.

## Introduction

Miniaturization processes requiring us to attain smaller and smaller devices and machines has prompted the development of organic electronics.[1] Organic photovoltaics (PV) play an important role in this field since they can act as efficient and clean energy sources for the independent operation of such devices.[2,3] The introduction of the bulk heterojunction concept

[†] Universidad Complutense de Madrid.
[‡] Eindhoven University of Technology.
[§] Universität Erlangen-Nürnberg.

(1) (a) Special Issue on Organic Electronics, *Chem. Mater.* **2004**, *16*, 4381−4846. (b) Wassel, R. A.; Gorman, C. B. *Angew. Chem., Int. Ed.* **2004**, *43*, 5120−5123. (c) Carroll, R. L.; Gorman, C. B. *Angew. Chem., Int. Ed.* **2002**, *41*, 4378−4400.

(2) For recent reviews on PV cells, see: (a) Brabec, C. J.; Sariciftci, N. S.; Hummelen, J. C. *Adv. Funct. Mater.* **2001**, *11*, 15−26. (b) Coakley, K. M.; McGehee, M. D. *Chem. Mater.* **2004**, *16*, 4533−4542. (c) Günes, S.; Neugebauer, H. *Chem. Rev.* **2007**, *107*, 1324−1338.

10.1021/jo702740d CCC: $40.75 
Published on Web 03/22/2008

for PV has provided a major boost in power conversion efficiencies, currently reaching values of 5% or more.[3] In those bulk heterojunction devices, the photoactive layer typically consists of a mixture of a $\pi$-conjugated semiconducting polymer, acting as p-type material, and a soluble $C_{60}$ derivative as the *n*-type material. A particular active strategy toward new PV designs is the molecular heterojunction.[4] Its foremost feature is incorporation in the photoactive layer of the device of $C_{60}$-based conjugates in which different electron donor moieties have been attached covalently to the fullerene cage. The close proximity of the photo- and electroactive units in such conjugates generally provides highly efficient photoinduced charge generation and can be tailored to exhibit long radical ion pair lifetimes.

Molecular heterojunction devices have been created by using a variety of $C_{60}$-based conjugates as the only photoactive material. First examples used oligo(*p*-phenylene vinylene)s (OPVs) of different lengths as donor molecules.[5,6] More recently, donor moieties such as oligothiophene, oligo(thienylene vinylene), and oligo(*p*-phenylene ethynylene) (OPE) $\pi$-conjugated oligomers, porphyrins, and $\pi$-extended tetrathiafulvalene derivatives have been applied in the fabrication of PV devices.[7] One of the drawbacks associated with most donor$-C_{60}$ conjugates reported to date is the relatively low content of fullerene in the final material, as compared to the more efficient polymer−fullerene blends, where the fullerene content is often as high as 80% by weight.[8]

Hence, in the search for new suitable $C_{60}$-based conjugates to construct efficient molecular-based PV devices, materials that possess a relatively high fullerene content seem to be favorable. In this regard, we recently reported the synthesis and PV application of a light-harvesting tetrafullerene nanoconjugate in which four $C_{60}$ units were covalently linked to a single OPE-type $\pi$-conjugated oligomer. Photophysical studies carried out in solution and in thin films demonstrated, however, that the observed low device performance was due to the absence of an efficient photoinduced electron-transfer process between the OPE central core and the peripheral $C_{60}$ units. The low tendency for photoinduced charge generation in these tetrafullerene conjugates was caused by a relatively high oxidation potential for the OPE oligomer. Nevertheless, the combination of this new conjugate as an electron acceptor with poly(3-hexylthiophene) (P3HT) as a donor led to devices that exhibited external quantum efficiencies of 15%.[9]

Herein, we take our first tetrafullerene prototype one step further to synthesize new tetrafullerene hybrids (**6** and **7**) whose redox and light-absorbing features were modulated finely by the introduction of thiophene rings on the periphery of the central core of the OPE or OPV trimers. Photophysical investigations, in solution and in film, were performed, and the corresponding all-organic solar cells were fabricated using these new conjugates as the only photoactive material and were compared to those using physical mixtures of the precursor aldehydes (**5a** and **5b)** with [$C_{60}$]PCBM.[10]

## Results and Discussion

**Synthesis.** Target arrays **6** and **7** were obtained by following a divergent multistep synthetic procedure using the previously described diformyl functionalized oligomers **1a** and **1b**.[11] The introduction of peripheral thiophene rings gives rise to new fluorophores and enhances the light-absorbing and redox properties of the final systems.[12] The peripheral functionalization toward the precursor aldehydes (**5a**,**b**) began with the corresponding bis(1,1-dibromovinylbenzene) derivatives (**2a**,**b**), which

(3) (a) Rowell, M. W.; Topinka, M. A.; McGehee, M. D.; Prall, H.-J.; Dennler, G.; Sariciftci, N. S.; Hu, L.; Gruner, G. *Appl. Phys. Lett.* **2006**, *88*, 233506/1−233506/3. (b) Sivula, K.; Luscombe, C. K.; Thompson, B. C.; Fréchet, J. M. J. *J. Am. Chem. Soc.* **2006**, *128*, 13988−13989. (c) Ma, W.; Yang, C.; Gong, X.; Lee, K.; Heeger, A. J. *Adv. Funct. Mater.* **2005**, *15*, 1617−1622. (d) Li, G.; Shrotriya, V.; Huang, J.; Yao, Y.; Moriarty, T.; Emery, K.; Yang, Y. *Nat. Mater.* **2005**, *4*, 864−868. (e) Riedel, I.; von Hauff, E.; Parisi, J.; Martín, N.; Giacalone, F.; Dyakonov, V. *Adv. Funct. Mater.* **2005**, *15*, 1979−1987. (f) Svensson, M.; Zhang, F.; Veenstra, S. C.; Verhees, W. J. H.; Hummelen, J. C.; Kroon, J. M.; Inganäs, O.; Andersson, M. R. *Adv. Mater.* **2003**, *15*, 988−991. (g) Wienk, M. M.; Kroon, J. M.; Verhees, W. J. H.; Knol, J.; Hummelen, J. C.; van Hal, P. A.; Janssen, R. A. J. *Angew. Chem., Int. Ed.* **2003**, *42*, 3371−3375. (h) Padinger, F.; Rittberger, R. S.; Sariciftci, N. S. *Adv. Funct. Mater.* **2003**, *13*, 1−4.

(4) For recent reviews on molecular heterojunction, see: (a) Roncali, J. *Chem. Soc. Rev.* **2005**, *34*, 483−495. (b) Segura, J. L.; Martín, N.; Guldi, D. M. *Chem. Soc. Rev.* **2005**, *34*, 31−47. (c) Nierengarten, J.-F. *New J. Chem.* **2004**, *28*, 1177−1191. (d) Nierengarten, J.-F. *Sol. Energy Mater. Sol. Cells* **2004**, *83*, 187−199. (e) Figueira-Duarte, T. M.; Gégout, A.; Nierengarten, J.-F. *Chem. Commun. (Cambridge, U.K.)* **2007**, 109−119.

(5) (a) Nierengarten, J.-F.; Eckert, J.-F.; Nicoud, J.-F.; Ouali, L.; Krasnikov, V.; Hadziioannou, G. *Chem. Commun. (Cambridge, U.K.)* **1999**, 617−618. (b) Eckert, J.-F.; Nicoud, J.-F.; Nierengarten, J.-F.; Liu, S.-G.; Echegoyen, L.; Barigelletti, F.; Armaroli, N.; Ouali, L.; Krasnikov, V.; Hadziioannou, G. *J. Am. Chem. Soc.* **2000**, *122*, 7467−7479.

(6) Peeters, E.; van Hal, P. A.; Knol, J.; Brabec, C. J.; Sariciftci, N. S.; Hummelen, J. C.; Janssen, R. A. J. *J. Phys. Chem. B* **2000**, *104*, 10174−10190.

(7) For oligo(phenylene ethynylene)$-C_{60}$ dyads, see: Gu, T.; Tsamouras, D.; Melzer, C.; Krasnikov, V.; Gisselbrecht, J.-P.; Gross, M.; Hadziioannou, G.; Nierengarten, J.-F. *ChemPhysChem* **2002**, *3*, 124−127. For oligothiophene$-C_{60}$ dyads, see: (a) Negishi, N.; Yamada, K.; Takimiya, K.; Aso, Y.; Otsubo, O.; Tetsuo, Y. *Chem. Lett.* **2003**, *32*, 404−405. (b) Negishi, N.; Takimiya, K.; Otsubo, T.; Harima, Y.; Aso, Y. *Synth. Met.* **2005**, *152*, 125−128. (c) Narutaki, M.; Takimiya, K.; Otsubo, T.; Harima, Y.; Zhang, H.; Araki, Y.; Ito, O. *J. Org. Chem.* **2006**, *71*, 1761−1768. For oligo(thienylene vinylene)$-C_{60}$ hybrids, see: (a) Guldi, D. M.; Luo, C.; Swartz, A.; Gómez, R.; Segura, J. L.; Martín, N.; Brabec, C.; Sariciftci, N. S. *J. Org. Chem.* **2002**, *67*, 1141−1152. (b) Negishi, N.; Yamada, K.; Takimiya, K.; Aso, Y.; Otsubo, T.; Harima, Y. *Chem. Lett.* **2003**, *32*, 404−405. (c) Handa, S.; Giacalone, F.; Haque, S. A., Palomares, E.; Martín, N.; Durrant, J. R. *Chem.*−*Eur. J.* **2005**, *11*, 7440−7447. For $C_{60}$−porphyrin conjugates, see: Imahori, H.; Fukuzumi, S. *Adv. Funct. Mater.* **2004**, *14*, 525−536. For $C_{60}$−tetrathiafulvalene triads, see: (a) Sánchez, L.; Sierra, M.; Martín, N.; Guldi, D. M.; Wienk, M. M.; Janssen, R. A. J. *Org. Lett.* **2005**, *7*, 1691−1694. (b) Kanato, H.; Narutaki, M.; Takimiya, K.; Otsubo, T.; Harima, Y. *Chem. Lett.* **2006**, *35*, 668−669.

(8) (a) Yu, G.; Gao, J.; Hummelen, J. C.; Wudl, F.; Heeger, A. J. *Science (Washington, DC, U.S.)* **1995**, *270*, 1789−1791. (b) Shaheen, S. E.; Brabec, C. J.; Sariciftci, N. S.; Padinger, F.; Fromherz, T.; Hummelen, J. C. *Appl. Phys. Lett.* **2001**, *78*, 841−843. (c) van Duren, J. K. J.; Yang, X. N.; Loos, J.; Bulle-Lieuwma, C. W. T.; Sieval, A. B.; Hummelen, J. C.; Janssen, R. A. J. *Adv. Funct. Mater.* **2004**, *14*, 425−434.

(9) Atienza, C. M.; Fernández, G.; Sánchez, L.; Martín, N.; Sá Dantas, I.; Wienk, M. M.; Janssen, R. A. J.; Rahman, G. M. A.; Guldi, D. M. *Chem. Commun. (Cambridge, U.K.)* **2006**, 514−516.

(10) Power conversion efficiencies of around 1% were recently reported by Roncali et al. for bulk heterojunction devices prepared from PCBM and different triphenylamine derivatives: (a) Roquet, S.; Cravino, A.; Leriche, P.; Alévêque, O.; Frère, P.; Roncali, J. *J. Am. Chem. Soc.* **2006**, *128*, 3459−3466. (b) Cravino, A.; Roquet, S.; Leriche, P.; Alévêque, O.; Frère, P.; Roncali, J. *Chem. Commun. (Cambridge, U.K.)* **2006**, 1416−1418.

(11) For the synthesis of the OPE-type trimer, see: Atienza, C.; Insuasty, B.; Seoane, C.; Martín, N.; Ramey, J.; Rahman, G. M. A.; Guldi, D. M. *J. Mater. Chem.* **2005**, *15*, 124−132. For the synthesis of the OPV-type trimer, see: Giacalone, F.; Segura, J. L.; Martín, N.; Guldi, D. M. *J. Am. Chem. Soc.* **2004**, *126*, 5340−5341.

(12) The substitution pattern, conjugation, and electronic structure of functionalized phenylacetylene and phenylvinylene structures are known to exhibit remarkable optical and electronic properties because of their multiple conjugated pathways. For recent examples, see: (a) Marsden, J. A.; Miller, J. J.; Shirtcliff, L. D.; Haley, M. M. *J. Am. Chem. Soc.* **2005**, *128*, 2464−2476. (b) Hwang, G. T.; Son, H. S.; Ku, J. K.; Kim, B. H. *J. Am. Chem. Soc.* **2003**, *125*, 11241−11248.

**SCHEME 1. Synthesis of Target Tetrafullerene Arrays 6 and 7**

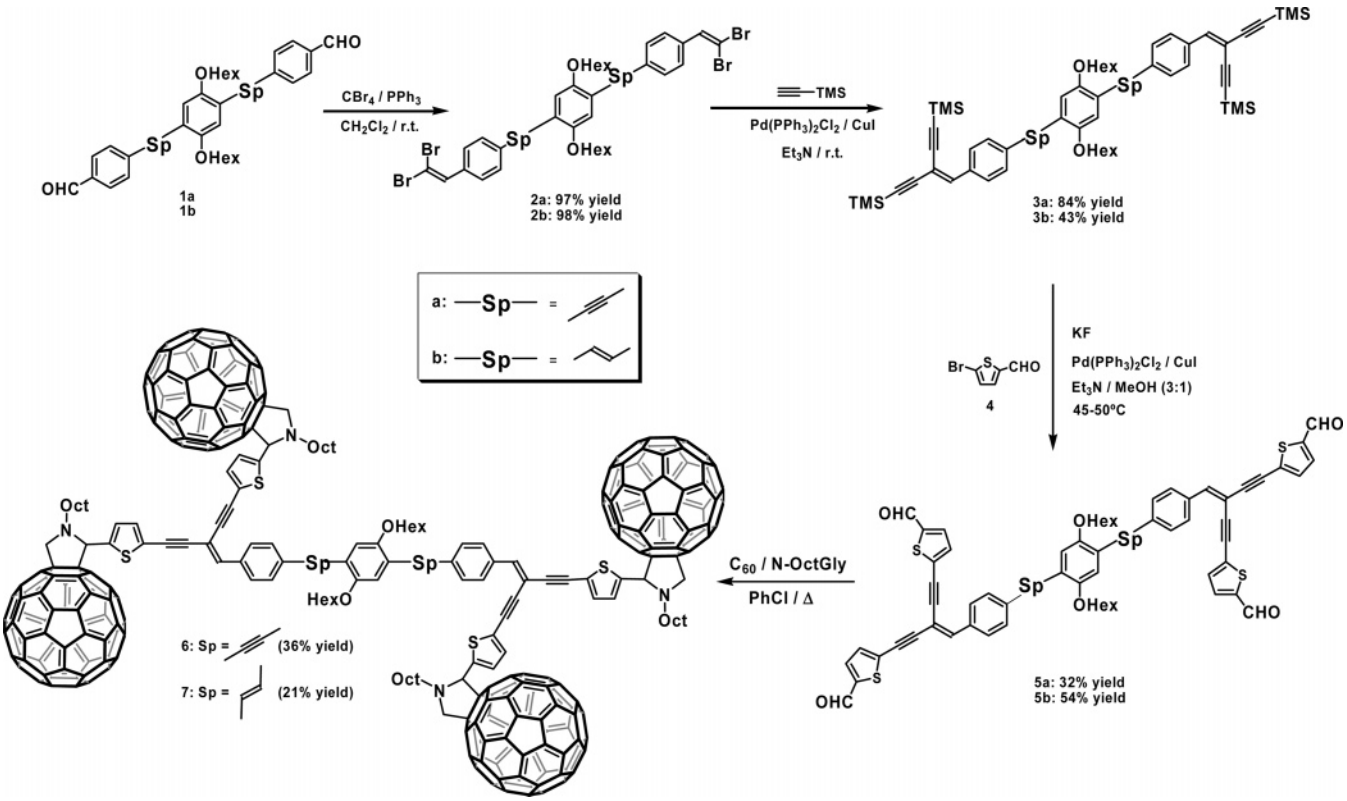


were readily obtained by reacting **1a** or **1b** with $CBr_4$ and $PPh_3$ following Corey and Fuch's method.[13] A Sonogashira cross-coupling reaction between **2** and (trimethylsilyl)acetylene led to the trimethylsilyl (TMS) derivatives **3a**,**b**.[14] In situ deprotection of their TMS groups with KF followed by a further 4-fold Sonogashira reaction with 2-bromo-5-formylthiophene (**4**) yielded the light-harvesting tetra-aldehydes **5a**,**b** as reddish solids. The last step toward the synthesis of target tetrafullerene arrays **6** and **7** was a 4-fold Prato 1,3-dipolar cycloaddition between the azomethine ylide—generated in situ by reacting *N*-octylglycine and the corresponding aldehyde—and one of the double bonds of the $C_{60}$. All the compounds reported herein were fully characterized through a wide variety of spectroscopic techniques (see Experimental Section and Supporting Information).

The $^1$H NMR spectra of **6** and **7** show only one set of resonances for each of the isochronous groups of protons. The resonances at $\delta$ ~5.4, 5.1, and 4.2 and also at $\delta$ ~4.1 corresponding to the pyrrolidine rings and to the $-O-CH_2-$ groups, respectively, are clear examples. These findings support the high symmetry of the final conjugates and, on the other hand, the lack of byproducts such as fullerene bis-adducts. At the same time, the absence of the signals at $\delta$ ~9.9 in the $^1$H NMR spectra and $\nu$ ~1660 cm$^{-1}$ in the FTIR spectra, diagnostic of the aldehyde functionality, rules out the presence of conjugates endowed with a lesser number of $C_{60}$ units. A comparative HPLC analysis of **6** and **7** supports this theory (see Figure S1).

**Optical Properties.** The light-absorbing features of all the compounds described in this study were investigated by UV–vis spectroscopy in chloroform. The increased conjugation

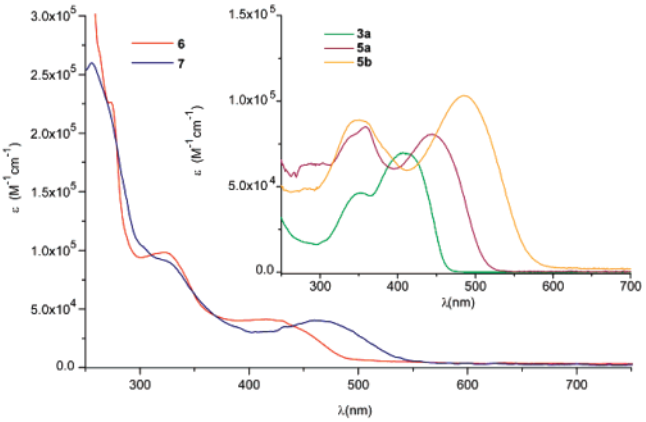


**FIGURE 1.** Absorption spectra of tetrafullerene conjugates **6** and **7** and precursors **3a**, **5a**, and **5b** (inset) in $CHCl_3$ at 298 K.

reached by the introduction of the peripheral thiophene rings in **5** in comparison to their TMS precursors **3** resulted in a significant bathochromic shift of the $\pi-\pi^*$ absorption band into the visible region of the solar spectrum (inset of Figure 1). Especially interesting is the case of tetra-aldehyde **5b**, in which the absorption maximum was observed at 492 nm ($\epsilon$ = 110 000 M$^{-1}$ cm$^{-1}$).

The decoration of the oligomeric core with fulleropyrrolidine moieties in hybrids **6** and **7** resulted in a slight reduction of the conjugation length as evidenced from both small hypsochromic shift and lower extinction coefficients in comparison to the precursor aldehydes (Figure 1). Additionally, both arrays **6** and **7** show an appreciable absorption in the UV region and a long tail covering the entire visible region up to ~700 nm.

**Cyclic Voltammetry (CV).** The redox characteristics of aldehydes **5a**,**b** and conjugates **6** and **7** were examined by CV

(13) Corey, E. J.; Fuchs, P. L. *Tetrahedron Lett.* **1972**, *13*, 3769–3772.
(14) Diederich, F.; Stang, P. J. *Metal-Catalyzed Cross-Coupling Reactions*; Wiley-VCH: Weinheim, Germany, 1998.

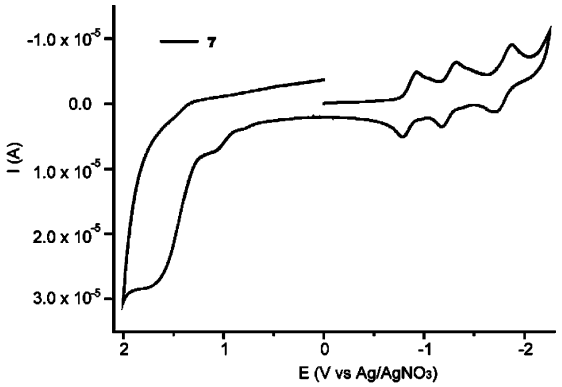


**FIGURE 2.** CV spectra of tetrafullerene array **7** in ODCB/MeCN (4:1), at room temperature and at 100 $mVs^{-1}$.

**TABLE 1. Redox Potential Values for Tetrafullerene Hybrids 6 and 7 and Their Precursors 5a,b**

| compd[a] | $E^1_{ox}$ | $E^2_{ox}$ | $E^3_{ox}$ | $E^1_{red}$ | $E^2_{red}$ | $E^2_{red}$ | $E^4_{red}$ |
|---|---|---|---|---|---|---|---|
| **5**a | +910 | +1130 | +1170 | −1410[b] | | | |
| **5**b | +860 | +1110 | +1560 | −1430[b] | | | |
| **6** | +810 | +1160 | +1640 | −950 | −1330 | −1890 | |
| **7** | +760 | +1020 | +1440 | −900 | −1290 | −1820 | |
| $C_{60}$ | | | | −760 | −1180 | −1650 | −2130 |

[a] Experimental conditions: mV vs $Ag/AgNO_3$, ODCB/$CH_3CN$ 4:1 as solvent, GCE as working electrode, Pt as counter-electrode, $Bu_4NClO_4$ (0.1 M) as supporting electrolyte, and scan rate of 100 mV $s^{-1}$. [b] Corresponding to the aldehyde functionality.

and differential pulse voltammetry (DPV) techniques in ODCB/MeCN (4:1) at room temperature (see Figure 2 for hybrid **7** and Table 1).

Concerning the electrochemical oxidation, the tetrafullerene hybrids (**6** and **7**) show three irreversible waves corresponding to the central $\pi$-conjugated oligomers. The first and second waves are quite weak, whereas the last one is very intense (Figure 2).[17] These findings are in agreement with the redox behavior observed for the precursor aldehydes **5**.[18] The incorporation of double bonds in the central oligomeric moiety in **5b** and **7** induces an anodic shift of the oxidation process in comparison with the OPE-type examples **5a** and **6** (see Table 1). These data confirm that the OPV spacer causes a lower oxidation potential in comparison to the OPE spacer and, hence, features stronger electron donating properties and a lower band gap.

The cyclic voltammograms of both hybrids **6** and **7** feature both oxidation and reduction waves that account for the amphoteric redox character of these samples. Regarding the electrochemical reduction, three quasi-reversible waves corresponding to the reduction of the fullerene cages appear. The presence of only one set of reduction waves points to the lack of interaction among the four $C_{60}$ units present in the molecule. As expected, the saturation of one of the double bonds of the fullerene units cathodically shifts those values as compared to pristine $C_{60}$ under the same experimental conditions.[15] All the reduction waves are accompanied by side waves that could be attributed to the adsorption of the measured compound over the electrode surface (see Figure 2).[16]

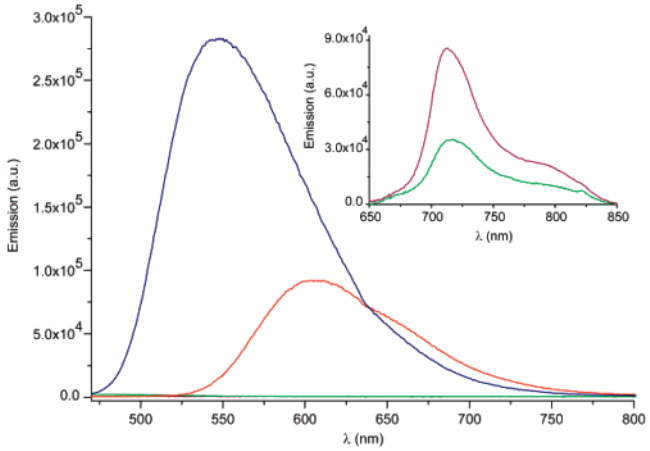


**FIGURE 3.** Room-temperature fluorescence spectra of the tetrafullerene conjugates **6** (purple) and **7** (green) together with those of the precursor aldehydes **5a** (blue) and **5b** (red) in THF recorded with solutions that exhibit optical absorptions at the 442 nm excitation wavelength of 0.2. The inset shows the fluorescence spectra of **6** (purple) and **7** (green) in the wavelength range of 650−800 nm.

**Photophysical Measurements in Solution.** The excited-state deactivation of the tetra-aldehydes **5a** and **5b** and conjugates **6** and **7** was examined by steady-state and time-resolved fluorescence spectroscopy in THF at room temperature. Considering the strongly fluorescing features of $\pi$-conjugated oligomers, the fluorescence of **5a**,**b** as reference systems was tested first. In accordance with the optical absorption, the fluorescence spectra of the tetra-aldehydes recorded with excitation at 442 nm show that the fluorescence maximum for **5a** (i.e., 545 nm) is blue-shifted as compared to that for **5b** (i.e., 604 nm). The fluorescence quantum yields of **5a** and **5b** are 0.31 and 0.14, respectively. The reduction in fluorescence quantum yield mainly is caused by an increased nonradiative decay as can be inferred from the fluorescence lifetimes for **5a** (i.e., 1.08 ns) and **5b** (i.e., 0.63 ns).

First insights into electron donor−acceptor interactions were gathered by comparing the fluorescence of **6** and **7** with that of **5a** and **5b** upon excitation at 442 nm, where the absorption was mainly that of the central core. Here, a significant quenching of the oligomeric fluorescence is observed (see Figure 3). Fluorescence quantum yields are $2 \times 10^{-3}$ for both conjugates **6** and **7**. The fluorescence is dual, that is, besides the oligomer relevant features in the 400−700 nm region, we see in the 650−800 nm range additional features similar to those seen for the fullerene fluorescence in *N*-methylfulleropyrrolidines.[19] If we compare the fluorescence quantum yields of the core unit to those of the corresponding aldehydes, we find that the quenching is about 2 orders of magnitude, implying that deactivation of the singlet state of the central chromophore occurs with a rate

(15) It is well-established that functionalization of the fullerene cage causes a rise of the LUMO energy level of the organofullerenes produced: Echegoyen, L.; Echegoyen, L. E. *Acc. Chem. Res.* **1998**, *31*, 593−601.

(16) Bard, A. J.; Faulkner, L. R. *Electrochemical Methods. Fundamentals and Applications*; John Wiley and Sons: New York, 2001.

(17) Unambiguous assignment of these weak waves to oxidative processes corresponding to the central $\pi$-conjugated oligomer was achieved using DPV measurements.

(18) Oxidation waves of $\pi$-conjugated oligomers sometimes appear as broad and difficult to assign waves in CV. For recent examples, see: (a) Zen, A.; Bilge, A.; Galbrecht, F.; Alle, R.; Meerholz, K.; Grenzer, J.; Neher, D.; Scherf, U.; Farrell, T. *J. Am. Chem. Soc.* **2006**, *128*, 3914−3915. (b) Narutaki, M.; Takimiya, K.; Otsubo, T.; Harima, Y.; Zhang, H.; Araki, Y.; Ito, O. *J. Org. Chem.* **2006**, *71*, 1761−1768. (c) Zhao, Y.; Shirai, Y.; Slepkov, A. D.; Cheng, L.; Alemany, L. B.; Sasaki, T.; Hegmann, F. A.; Tour, J. M. *Chem.—Eur. J.* **2005**, *11*, 3643−3658.

(19) Atienza, C.; Martín, N.; Wielopolski, M.; Haworth, N.; Clark, T.; Guldi, D. M. *Chem. Commun. (Cambridge, U.K.)* **2006**, 3202−3204.

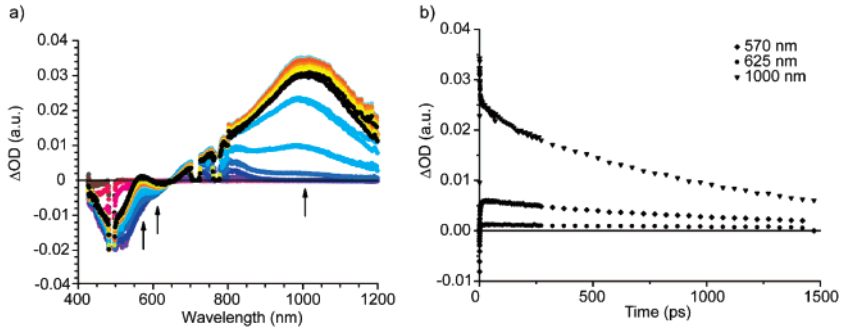


**FIGURE 4.** (a) Selected differential absorption spectra (visible and near-IR) obtained upon femtosecond photoexcitation (490 nm) of **5b** in nitrogen saturated THF solutions with several time delays between 0 and 1500 ps at room temperature and (b) time−absorption profiles of the spectra at 570, 625, and 1000 nm, monitoring the decay of the **5b** singlet excited state.

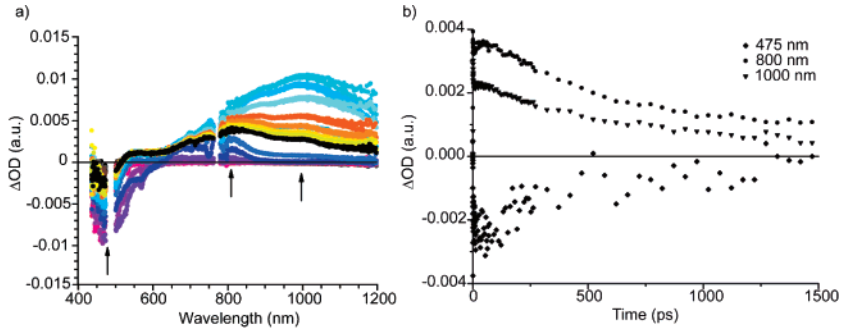


**FIGURE 5.** (a) Selected differential absorption spectra (visible and near-IR) obtained upon femtosecond photoexcitation (490 nm) of **7** in nitrogen saturated THF solutions with several time delays between 0 and 1500 ps at room temperature and (b) time−absorption profiles of the spectra at 475, 800, and 1000 nm, monitoring the formation and decay of the radical ion pair state.

constant that is 100 times faster than in the corresponding aldehydes and hence occurs in the range of 10 ps. The quantum yields of the fullerene part of the fluorescence (i.e., $5 \times 10^{-4}$ and $3 \times 10^{-4}$ for **6** and **7**, respectively) are lower than found for *N*-methylfulleropyrrolidine (MP−$C_{60}$) (i.e., $6.0 \times 10^{-4}$) but show nevertheless that, eventually, a large fraction (50−80%) of the absorbed photons in **6** and **7** end up producing the $C_{60}$ singlet excited state. Hence, in solution, an energy-transfer process takes place after photoexcitation of the cores of hybrids **6** and **7**.

To elucidate the intramolecular electron donor−acceptor interactions, we carried out time-resolved transient absorption measurements, following pulsed photoexcitation, for the starting aldehydes **5a** and **5b** as well as the corresponding tetrafullerene nanoconjugates **6** and **7**. Representative femtosecond time-resolved absorption spectra for **5b** dissolved in THF, taken after a 150 fs laser pulse at 490 nm, are displayed in Figure 4. The corresponding spectra for **5a** are shown as Figure S2. The differential spectrum recorded immediately after the laser pulse was characterized by bleaching of the ground-state absorption at 485 nm as well as a broad absorption between 530 and 1200 nm. These spectral attributes are indicative of the **5b** singlet excited state, which decays slowly ($4.9 \times 10^8$ $s^{-1}$) to the energetically lower-lying triplet excited state predominantly via intersystem crossing. The triplet excited state features absorption maxima between 630 and 830 nm.[20] Similar, although 2 times faster, is the decay of the **5a** singlet excited state ($9.8 \times 10^8$ $s^{-1}$) forming the corresponding triplet manifold.[21]

The transient absorption changes of tetrafullerene **6** (Figure S3) and **7** (Figure 5) were also recorded in THF with several time delays after a 490 nm femtosecond laser pulse, and these can be compared to what was seen for the **5a** and **5b** references. At early times (i.e., 5−10 ps), these are practically identical to those of the references, disclosing strong bleaching at 485 nm and a broad absorption between 530 and 1200 nm, which is attributed to absorption of the singlet excited state of the conjugated core. Since energy transfer to $C_{60}$ is known to proceed at time scales of 200 fs or less,[22] this broad transient band between 430 and 1200 nm also can be partly due to the singlet excited-state absorption of $C_{60}$, which is known to occur between 750 and 1150 nm, with a maximum at 960 nm.[23]

At a delay time of 100 ps (Figure 5), a new transition that covers most of the visible range, and centered at 800 nm, grows in, accompanied by another absorption in the near-IR range at about 1000 nm. We ascribe the former to the $\pi$-radical cation of the conjugated core, while the latter band belongs to the fullerene $\pi$-radical anion.[24] Support for the $\pi$-radical cation assignment came from pulse radiolysis studies following the one-electron oxidation of **5a** and **5b**.

The spectral changes for **5b** are exemplified in Figure 6 and reflect a good agreement with the transient absorption changes

(20) Peeters, E.; Marcos, A.; Meskers, S. C. J.; Janssen, R. A. J. *J. Chem. Phys.* **2000**, *112*, 9445−9454.

(21) We note that, especially for **5b**, the lifetime of the singlet excited state inferred from transient absorption and fluorescence spectroscopy is different. Since the fluorescence can be measured very sensitively over several orders of magnitude and over a longer time period, these values are likely more accurate.

(22) (a) van Hal, P. A.; Janssen, R. A. J.; Lanzani, G.; Cerullo, G.; Zavellani-Rossi, M.; De Silvestri, S. *Phys. Rev. B: Condens. Matter Mater. Phys.* **2001**, *64*, 75206/1−75206/7. (b) van Hal, P. A.; Janssen, R. A. J.; Lanzani, G.; Cerullo, G.; Zavellani-Rossi, M.; De Silvestri, S. *Chem. Phys. Lett.* **2001**, *345*, 33−38.

(23) Watanabe, A.; Ito, O.; Watanabe, M.; Saito, H.; Koishi, M. *Chem. Commun. (Cambridge, U.K.)* **1996**, 117−118.

(24) Guldi, D. M.; Maggini, M.; Scorrano, G.; Prato, M. *J. Am. Chem. Soc.* **1997**, *119*, 974−980.

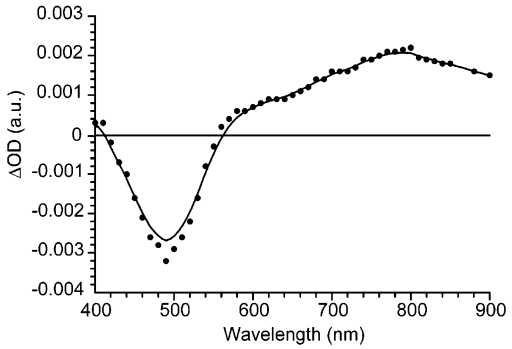


**FIGURE 6.** Differential absorption changes (visible) following pulse radiolytic oxidation of **5b** in oxygenated dichloromethane with $^{\bullet}OOCH_2$-Cl or $^{\bullet}OOCHCl_2$ radicals.

**TABLE 2. Device Properties, Short Circuit Current Density ($J_{SC}$), Open Circuit Voltage ($V_{OC}$), Fill Factor (FF), Estimated Efficiency ($\eta$), and Film Thickness of PV Devices with Device Structure Glass/ITO/PEDOT:PSS/Active Layer/LiF/Al**

| active layer (ratio) | $J_{SC}$ (mA cm$^{-2}$) | $V_{OC}$ (V) | FF | $\eta^a$ | $d$ (nm) |
|---|---|---|---|---|---|
| **6** | 0.04 | 0.42 | 0.28 | 0.005 | 64 |
| **7** | 0.27 | 0.21 | 0.25 | 0.015 | 37 |
| **5a**/PCBM (1:4) | 0.10 | 0.12 | 0.25 | 0.003 | 67 |
| **5b**/PCBM (1:4) | 2.04 | 0.40 | 0.26 | 0.214 | 50 |

[a] Efficiency ($\eta$) was not corrected for emission profile of tungsten test lamp.

upon photoexcitation of **7**, revealing a broad absorption with a maximum at 800 nm. In accordance with these results, we propose that in **6** and **7**, electron transfer from the core to the electron accepting fullerene creates the radical ion pair state. The transfer reaction is responsible for the fast deactivation of the photoexcited chromophores. Analyzing the absorption time profiles, we derived rate constants of $3.0 \times 10^{10}$ s$^{-1}$ either for **6** or for **7** for the intramolecular charge separation.

The radical ion pair state is, however, short-lived and decays with rate constants of $4.6 \times 10^8$ and $9.7 \times 10^8$ s$^{-1}$ for **6** and **7**, respectively. Products of these charge recombination processes in both nanoarrays (**6** and **7**) are partly the singlet fullerene excited state, as evidenced by the fluorescence quantum yields that are 50−80% of the *N*-methylfulleropyrrolidine (MP−$C_{60}$) used as the reference. This singlet excited state decays predominantly via intersystem crossing to the fullerene triplet as evidenced by the characteristic triplet−triplet absorption at 700 nm, −which is seen to decay on the microsecond time scale (Figure S4).

**PV Devices.** Four types of PV devices were prepared comprising different photoactive layers, that is, nanoconjugate **6**, nanoconjugate **7**, and blends of aldehydes **5a** and **5b** with [$C_{60}$]PCBM. The blends with PCBM contain the same ratio as the conjugates: one aldehyde molecule per four PCBM molecules. All devices gave a modest PV response (Table 2 and Figure S5), exhibiting low fill factors (FF = 0.25−0.30) and open circuit voltages ($V_{OC}$ = 0.1−0.4 V). The relation between $V_{OC}$ and oxidation potentials in these cells is not linear. This is mainly due to fact that the best performance was for thin layers (Table 2), in which $V_{OC}$ not only was determined by the energy levels of the molecules but also by the balance between photocurrent and leakage current. The main differences in device performance between the studied active layers stem from the short circuit current density ($J_{SC}$). For both nanoconjugates, $J_{SC}$ is well below 1 mA cm$^{-2}$, with that of **7** (0.27 mA cm$^{-2}$) being 6 times higher than that of **6**. The low current is consistent with the rapid charge recombination process described in the previous section. The difference between the two nanoconjugates can be explained partially by the fact that the absorption of 7 extends further into the visible region, and hence, more photons are absorbed. Additionally, **7** features a stronger electron donor capability than **6**, which may impact charge generation and device performance positively. Also, in the blends with PCBM, the device containing the OPV donor (aldehyde **5b**) performs much better than that with the OPE donor (aldehyde **5a**), the former having an appreciable $J_{SC}$ value of 2.04 mA cm$^{-2}$, resulting in an estimated light to electrical power conversion efficiency of 0.21%. The external quantum efficiency of this cell amounts to 15−20% in the absorption band (350−550 nm). Using the absorbance $A = 0.15$ of the 50 nm film in this range, 0.5 ($1-10^{-2A}$) is an upper limit for the fraction of absorbed photons, resulting in an internal quantum efficiency of about 30−40%. Considering the rapid recombination rate and modest behavior of nanoconjugate **7**, the good performance of the **5b**/PCBM blend indicates the importance of phase separation. Apparently, the larger phase separation that is likely present in the blend as compared to the well-defined nanoconjugates is a requirement for the generation of free charge carriers. Phase separation enables charges to be separated over longer distances, reducing their probability to recombine. Nevertheless, also in the **5b**/PCBM blend, the majority (60−70%) of charge carriers that are formed recombine before they can be collected. Apart from fast geminate recombination, a low hole mobility in these compounds is most probably responsible for the observed recombination and is consistent with the low fill factors.

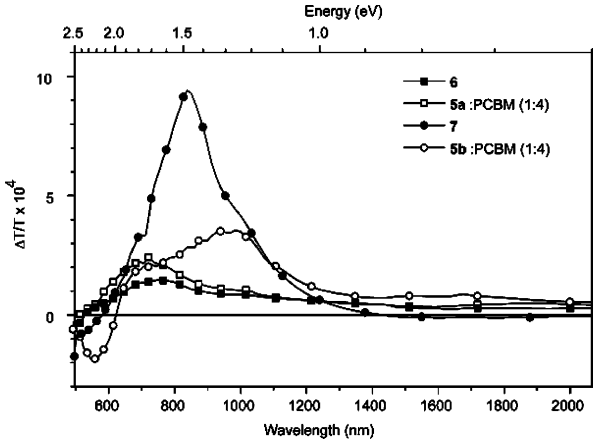


**FIGURE 7.** Near steady-state photoinduced absorption spectra of drop-cast films of **6** and **7** and blends of **5a** and **5b** with PCBM on quartz. The samples were kept at 80 K and photoexcited at 488 nm with a 50 mW laser, modulated with 275 Hz.

**Photophysical Measurements in Thin Films.** Near steady-state photoinduced absorption (PIA) spectra on thin films can give further insight into the processes that occur upon photoexcitation of the photoactive layers. The PIA spectra (Figure 7) of the films incorporating the OPE chromophore (**5a**/PCBM and **6)** are very similar to the spectra of **6** in THF (Figure S3) at long delay times. The main contribution to the absorption is that of the fullerene triplet state, having a maximum at 720 nm (1.72 eV) and a lifetime of 50 $\mu$s, typical for that of the $C_{60}$ excited triplet state. Apparently, the photoexcitation ends up at the $C_{60}$ excited triplet state, such as in the THF solution (see Figure S4). This is consistent with the low photocurrent observed

in the corresponding PV devices. The spectra of **7** and the blend of **5b** with PCBM are more difficult to interpret (Figure 7). The spectrum of the blend has a broad absorption from 600 to 1200 nm with a peak at 960 nm and a shoulder at 700 nm. In addition, there is a weak absorption in the infrared portion of the spectrum (1750 nm). We attribute the absorptions to a superposition of the absorption of the radical cation of **5b**— with one broad band similar to that in Figure 6 and a maximum at 800 nm and one less intense band at low energy (1750 nm)— and the radical anion of PCBM at around 1000 nm. The main feature of the spectrum of **7** is the absorption at 840 nm, about 100 nm red-shifted from the triplet absorption spectrum of the aldehyde in solution (Figure 4). To explain the strong 840 nm absorption and the concurrent absence of a band above 1300 nm in the PIA spectrum of **7**, we assign it to the triplet state of the conjugated core of **7**. Previously, it was shown that for linear dialkoxy-OPVs, the triplet-state energy of an OPV segment endowed with three double bonds and four phenyl rings is equal to the triplet-state energy of MP−$C_{60}$ (1.5 eV) and lower for longer derivatives.[25] Therefore, the triplet energy may be transferred from the fullerene back to the oligomer, an effect that has been observed previously for other systems.[26] This explanation is in good agreement with the lower photocurrent found for **7** as compared to the **5b**/PCBM blend. The blend— for which the triplet state is not extensively populated—showed a 20-fold better performance than nanoconjugate **7**. The different behavior of **7** and the blend of **5b** and PCBM can be rationalized assuming that phase separation is not only beneficial for charge transport but also affects the energy levels of electrons and holes in such a way that it favors charge separation and prevents recombination. If the holes and electrons cannot be transported from the molecular heterojunction at which they were created, recombination to the ground state or to a suitably positioned triplet state is inevitable. The chance for the photogenerated hole hopping into a donor domain is much larger for the **5b**/PCBM blend than for nanoconjugate **7**.

## Conclusion

We synthesized and characterized two new hybrids comprising conjugated OPE and OPV segments and four dangling fullerenes and investigated their behavior as molecular heterojunctions with transient optical spectroscopy and by preparing PV devices. In solution, these nanoconjugates exhibit a very fast (∼10 ps) deactivation of the singlet excited state of the core unit that produces a mixture of a charge-separated state, involving a radical cation on the $\pi$-conjugated oligomer and the fullerene anion at one of the termini, and a local fullerene singlet excited state. Formation of the charge-separated state is more pronounced for **7**, whose central core presents a stronger donor character. Subsequently, the charge-separated state recombines to the $C_{60}$ singlet state and then produces, via intersystem crossing, the $C_{60}$ triplet state. In the solid state, the final outcome is slightly different for **7**, where the preferred long-lived excited state is a triplet OPV core. As both nanohybrids **6** and **7** do not form long-lived charge carriers in thin films, the photocurrent observed in the corresponding PV devices is limited. When the same chromophores OPE and OPV aldehydes **5a** and **5b** are physically mixed with PCBM as an acceptor, the photophysical processes change partially. For the OPV aldehyde, we now observe the formation of long-lived charges in the PIA experiment and at the same time are able to collect a reasonably high photocurrent of 2 mA $cm^{-2}$. These changes between the nanoconjugates and the physical blends are tentatively attributed to an improved charge separation after charge generation as a result of partial aggregation of either or both of the components that enables charges to dissociate from the initial location where they were generated. Hence, the size of the donor and acceptor domains that can be created is an important parameter for the design of new covalently linked donor−acceptor systems, such as block copolymers, for PV applications.

## Experimental Section

**Compound 2b.** To a solution of $CBr_4$ (5.04 g, 15.22 mmol) and $PPh_3$ (7.98 g, 30.44 mmol) in dry $CH_2Cl_2$ (60 mL) was added at once **1b** (2.05 g, 3.80 mmol). The resulting mixture was stirred at room temperature for 2 h, washed with water, and dried over $MgSO_4$. Upon filtration, the solvent was evaporated, and the crude product was purified by column chromatography [$SiO_2$, hexane/dichloromethane (1:1)] to afford **2b** (3.2 g, 98%) as an orange solid. $^1$H NMR ($CDCl_3$, 300 MHz): $\delta$ 7.54 (m, 12 H), 7.15−7.09 (m, 4H), 4.07 (t, $J$ = 6.4 Hz, 4H), 1.89 (m, 4H), 1.57 (m, 4H), 1.46−1.33 (m, 8H), 0.94 (t, $J$ = 6.8 Hz, 6H). $^{13}$C NMR ($CDCl_3$, 75 MHz) $\delta$ 151.6, 138.6, 136.9, 134.5, 129.1, 128.4, 127.2, 126.8, 124.8, 110.9, 89.4, 69.9, 32.0, 29.8, 26.3, 23.0, 14.4. FTIR (KBr): $\nu$ 3042, 2982, 1660, 1282, 1218, 832, 810 $cm^{-1}$. UV−vis ($CHCl_3$): $\lambda_{max}$ ($\epsilon$) 344 (27 500), 413 (40 000) nm. ESI-MS $m/z$: 847.1 [M + $H^+$].

**Compound 3a.** To a solution of **2a** (300 mg, 0.35 mmol) in $Et_3N$ (15 mL), $Pd(PPh_3)_2Cl_2$ (49.7 mg, 0.07 mmol), CuI (7 mg, 0.035 mmol), and (trimethylsilyl)acetylene (0.4 mL, 2.8 mmol) were added. The resulting mixture was stirred for 2 h, the solvent was evaporated to dryness, and the crude product was purified by column chromatography [$SiO_2$, hexane/dichloromethane (3:1)] to afford **3a** (270 mg, 84%) as a yellow solid. $^1$H NMR ($CDCl_3$, 300 MHz): $\delta$ 7.70 (dd, $J$ = 8.4 Hz, 8H), 7.07 (s, 2H), 7.02 (s, 2H), 4.04 (t, $J$ = 6.4 Hz, 4H), 1.91−1.81 (m, 4H), 1.60−1.53 (m, 4H), 1.40−1.25 (m, 8H), 0.93−0.88 (t, 6H), 0.29 (s, 18H), 0.25 (s, 18H). $^{13}$C NMR ($CDCl_3$, 75 MHz): $\delta$ 153.9, 144.4, 135.4, 132.7, 131.6, 131.4, 129.1, 124.4, 117.0, 114.2, 104.2, 103.9, 102.3, 101.8, 95.2, 94.3, 88.1, 69.8, 32.1, 29.8, 25.8, 22.7, 14.4, 0.0, −0.25. FTIR (KBr) $\nu$ 2956, 2937, 2148, 1629, 1598, 1514, 1250, 1218, 889, 844, 760, 698, 626, 540 $cm^{-1}$. UV−vis ($CHCl_3$): $\lambda_{max}$ ($\epsilon$) 352 (46 000), 407 (70 000) nm. ESI-MS $m/z$: 915.5 [M + $H^+$].

**Compound 3b.** To a solution of **2b** (1 g, 1.176 mmol) in $Et_3N$ (30 mL), $Pd(PPh_3)_2Cl_2$ (206 mg, 0.294 mmol), CuI (22 mg, 0.1176 mmol), and (trimethylsilyl)acetylene (1.32 mL, 9.4 mmol) were added. The resulting mixture was stirred for 10 h, the solvent was evaporated to dryness, and the crude product was purified by column chromatography [$SiO_2$, hexane/dichloromethane (5:1)] to afford **3b** (460 mg, 43%) as a orangish solid. $^1$H NMR ($CDCl_3$, 300 MHz) $\delta$ 7.91 (d, $J$ = 8.46 Hz, 4H), 7.57 (s, 1H), 7.51 (s, 1H), 7.50 (d, $J$ = 8.3 Hz, 4H), 7.17 (s, 1H), 7.13 (m, 3H), 7.08 (s, 2H), 4.07 (t, $J$ = 6.3 Hz, 4H), 1.89 (m, 4H), 1.56 (m, 4H), 1.40 (m, 8H), 0.93 (t, $J$ = 6.8 Hz, 6H), 0.28 (s, 18H), 0.24 (s, 18H). $^{13}$C NMR ($CDCl_3$, 75 MHz) $\delta$ 151.6, 145.24, 139.4, 134.9, 130.0, 128.6, 127.3, 126.6, 110.9, 104.7, 102.8, 102.3, 102.1, 94.0, 69.9, 32.0, 29.8, 26.3, 23.0, 14.4, 0.3, 0.07. FTIR (KBr) $\nu$ 3026, 2970, 2923, 1602, 1216, 756, 667 $cm^{-1}$. UV−vis ($CHCl_3$) $\lambda_{max}$ ($\epsilon$) 350 (16 000), 438 (29 000) nm. ESI-MS $m/z$: 916.6 [M + $H^+$].

**Compound 5a.** To a solution of **3a** (320 mg, 0.355 mmol) and 5-bromothiophene-2-carboxaldehyde (0.42 mL, 3.52 mmol) in $Et_3N$/MeOH (3:1) (20 mL) under Ar atmosphere, KF (164 mg, 2.83

(25) van Hal, P. A.; Beckers, E. H. A.; Apperloo, J. J.; Janssen, R. A. J. *Chem. Phys. Lett.* **2000**, *348*, 403−408.

(26) (a) van Hal, P. A.; Knol, J.; Langeveld-Voss, B. M. W.; Meskers, S. C. J.; Hummelen, J. C.; Janssen, R. A. J. *J. Phys. Chem. A* **2000**, *104*, 5974−5988. (b) Schüppel, R.; Uhrich, C.; Pfeiffer, M.; Leo, K.; Brier, E.; Reinold, E.; Bäuerle, P. *ChemPhysChem* **2007**, *8*, 1497−1503.

mmol), $Pd(PPh_3)_2Cl_2$ (50 mg, 0.07 mmol), and CuI (6.8 mg, 0.035 mmol) were added. The resulting solution was stirred overnight at room temperature. The solvent was evaporated to dryness, and the crude product was purified by column chromatography [$SiO_2$, chloroform/methanol (20:1)] to afford **5a** (120 mg, 32%) as an orange solid. $^1$H NMR ($CDCl_3$, 300 MHz) $\delta$ 9.92 (s, 2H), 9.90 (s, 2H), 7.74 (dd, $J$ = 8.4 Hz, 8H), 7.72 (dd, $J$ = 3.9 Hz, 4H), 7.39 (dd, $J$ = 3.9 Hz, 4H), 7.28 (s, 2H), 7.05 (s, 2H), 4.06 (t, $J$ = 6.4 Hz, 4H), 1.92−1.83 (m, 4H), 1.65−1.52 (m, 4H), 1.43−1.26 (m, 8H), 0.89 (t, $J$ = 6.8 Hz, 6H). $^{13}$C NMR (DMSO-$d_6$, 75 MHz) $\delta$ 185.1, 154.1, 144.3, 139.8, 138.9, 138.6, 137.5, 137.0, 135.5, 134.9, 134.8, 134.7, 132.9, 132.4, 132.3, 131.4, 131.3, 130.9, 130.3, 129.1, 128.7, 80.2, 80.0, 79.8, 61.5, 55.7, 32.1, 29.8, 29.5, 26.3, 26.1, 22.9, 14.8. FTIR (KBr) $\nu$ 2922, 2852, 2200, 1662, 1598, 1456, 1217, 777, 756, 669 cm$^{-1}$. UV−vis ($CHCl_3$) $\lambda_{max}$ ($\epsilon$) 360 (83 400), 443 (88 500) nm. ESI-MS $m/z$: 1066.2 [M + H$^+$].

**Compound 5b.** To a solution of **3b** (430 mg, 0.467 mmol) and 5-bromothiophene-2-carboxaldehyde (0.55 mL, 4.64 mmol) in $Et_3N$/MeOH (3:1) (40 mL) under Ar atmosphere, KF (217 mg, 3.74 mmol), $Pd(PPh_3)_2Cl_2$ (65 mg, 0.093 mmol), and CuI (9 mg, 0.047 mmol) were added. The resulting solution was stirred overnight at room temperature. The solvent was evaporated to dryness, and the crude product was purified by column chromatography [$SiO_2$, chloroform] to afford **5b** (270 mg, 54%) as a dark-red solid. $^1$H NMR ($CDCl_3$, 300 MHz) $\delta$ 9.92 (s, 2H), 9.89 (s, 2H), 7.90 (d, $J$ = 8.4 Hz, 4H), 7.72 (dd, $J$ = 3.9 Hz, 4H), 7.61−7.57 (m, 6H), 7.39 (dd, $J$ = 3.8 Hz, 4H), 7.29 (s, 2H), 7.22 (s, 1H), 7.17−7.15 (m, 3H), 4.10 (t, $J$ = 6.4 Hz, 4H), 1.91 (m, 4H), 1.57 (m, 4H), 1.41 (m, 8H), 0.93 (br t, $J$ = 6.9 Hz, 6H). $^{13}$C NMR ($CDCl_3$, 75 MHz) $\delta$ 183.0, 182.8, 151.7, 146.4, 145.2, 144.6, 144.2, 140.5, 137.4, 136.4, 134.9, 134.8, 134.7, 134.4, 133.5, 133.3, 132.6, 132.1, 131.4, 130.7, 130.3, 128.8, 128.7, 128.6, 128.5, 128.4, 127.3, 127.1, 126.9, 125.8, 111.06, 100.8, 97.0, 94.9, 88.3, 82.3, 69.9, 32.0, 30.1, 29.8, 26.3, 23.0, 14.4. FTIR (KBr) $\nu$ 3053, 3022, 2925, 2854, 2194, 1668, 1595, 1425, 1220, 1197, 808, 721, 694, 669, 578, 542 cm$^{-1}$. UV−vis ($CHCl_3$) $\lambda_{max}$ ($\epsilon$) 336 (94 600), 492 (110 000) nm. ESI-MS $m/z$: 1070.3 [M + H$^+$].

**Compound 6.** A solution of **5a** (100 mg, 0.09 mmol), *N*-octylglycine (101 mg, 0.56 mmol), and $C_{60}$ (541 mg, 0.75 mmol) in chlorobenzene (50 mL) was heated under reflux overnight. The solvent was evaporated to dryness, and the crude product was purified by column chromatography [$SiO_2$, $CS_2$, chloroform] to afford **6** (150 mg, 36%) as a black solid. $^1$H NMR ($CDCl_3$, 300 MHz) $\delta$ 7.67 (dd, $J$ = 8.6 Hz, 8H), 7.35−7.20 (m, 8H), 7.08 (s, 2H), 6.95 (s, 2H), 5.38 (br s, 4 H), 5.12 (d, $J$ = 9.4 Hz, 4H), 4.12 (d, $J$ = 9.4 Hz, 4H), 4.02−3.98 (br t, $J$ = 6.4 Hz, 4H), 3.5−3.36 (m, 30 H), 2.72−0.78 (m, 60 H). $^{13}$C NMR ($CDCl_3$, 125 MHz) $\delta$ 55.7, 153.7, 153.6, 153.5, 153.4, 153.3, 152.7, 152.7, 152.63, 152.60, 147.1, 146.56, 146.50, 146.2, 146.1, 146.0, 145.99, 145.92, 145.8, 145.7, 145.6, 145.58, 145.51, 145.39, 145.31, 145.2, 145.18, 145.15, 145.12, 145.07, 145.02, 144.9, 144.6, 144.55, 144.52, 144.3, 144.2, 144.14, 144.10, 143.9, 143.8, 143.4, 143.0,142.8, 142.5, 142.43, 142.40, 142.2, 142.1, 142.0, 141.98, 141.92, 141.88, 141.83, 141.7, 141.6, 141.9, 141.4, 140.0, 139.8, 139.6, 137.0, 136.4, 135.7, 135.3, 135.0, 132.1, 131.8, 131.7, 131.4, 128.79, 128.73, 127.9, 127.8, 127.77, 127.70, 124.3, 124.2, 123.9, 123.7, 116.5, 78.0, 69.3, 69.2, 68.3, 66.8, 32.05, 32.01, 31.6, 29.7, 29.48, 29.40, 28.4, 27.6, 25.8, 22.91, 22.88, 22.83, 14.3, 14.1. FTIR (KBr) $\nu$ 2920, 2850, 2187, 1596, 1463, 1210, 758, 526 cm$^{-1}$. UV−vis ($CHCl_3$) $\lambda_{max}$ ($\epsilon$) 322 (147 000), 426 (60 000) nm. MALDI-TOF MS $m/z$: 4446.4 [M$^+$].

**Compound 7.** A solution of **5b** (170 mg, 0.16 mmol), *N*-octylglycine (172 mg, 0.95 mmol), and $C_{60}$ (914 mg, 1.27 mmol) in chlorobenzene (50 mL) was heated under reflux overnight. The solvent was evaporated to dryness, and the crude product was purified by column chromatography [$SiO_2$, $CS_2$, chloroform] to afford **7** (150 mg, 21%) as a black solid. $^1$H NMR ($D_2O$, 300 MHz) $\delta$ 7.92 (br d, 4H), 7.54−7.05 (m, 20H, Ar), 5.45 (br s, 4H), 5.18 (br s, 4H), 4.22 (br s, 4H), 4.10 (br t, 4H), 3.54−3.08 (m, 34H), 2.73−0.99 (m, 60H). $^{13}$C NMR ($D_2O$, 75 MHz) $\delta$ 156.2, 155.5, 154.3, 154.2, 153.39, 153.32, 153.27, 153.22, 153.1, 151.6, 147.8, 147.29, 147.25, 146.94, 146.91, 146.84, 146.80, 146.78, 146.73, 146.65, 146.62, 146.5, 146.4, 146.3, 146.28, 146.23, 146.1, 146.04, 146.02, 146.00, 145.84, 145.80, 145.7, 145.3, 145.27, 145.24, 145.1, 144.9, 144.1, 143.7, 143.6, 143.5, 143.4, 143.3, 143.1, 142.8, 142.7, 142.6, 142.5, 142.4, 142.3, 142.25, 142.22, 140.8, 140.6, 140.45, 140.43, 137.7, 137.29, 137.2, 136.9, 136.4, 136.1, 135.2, 132.7, 132.2, 131.8, 130.2, 128.7, 128.5, 128.3, 127.4, 127.2, 125.4, 125.2, 124.8, 110.6, 102.7, 97.1, 95.2, 94.2, 92.9, 89.8, 89.2, 83.8, 78.9, 77.7, 77.2, 77.0, 76.9, 71.1, 69.6, 69.0, 68.5, 67.6, 55.7, 54.4, 33.1, 33.0, 32.7, 30.8, 30.5, 29.5, 28.6, 27.1, 24.1, 24.0, 15.4, 15.3. FTIR (KBr) $\nu$ 2920, 2850, 2180, 1595, 1463, 1178, 1114, 810, 769, 758, 526 cm$^{-1}$. UV−vis ($CHCl_3$) $\lambda_{max}$ ($\epsilon$) 255 (257 000), 325 (92 500), 467 (40 000) nm. MALDI-TOF MS $m/z$: 4450.6 [M$^+$].

**Acknowledgment.** Financial support from the MCyT of Spain and Comunidad de Madrid (Projects BQU2002-00855 and P-PPQ-000225-0505), the EU (RTN network "WONDERFULL" and "CASSIUS CLAYS", and NAIMO Integrated Project NMP4-CT-2004-500355), SFB 583, DFG(GU 517/4-1), FCI, and the Office of Basic Energy Sciences of the U.S. Department of Energy (NDRL-5000) is gratefully acknowledged. G.F. thanks MEC for a research grant. Anne-Sophie Dupain is thanked for help with the preparation of PV devices.

**Supporting Information Available:** General methods, additional Figures S1−4, and copy of $^1$H and $^{13}$C NMR spectra. This material is available free of charge via the Internet at http://pubs.acs.org.

JO702740D